J. Fluid Mech. (1995), *vol.* 283, *pp.* 273–285

Three-dimensional calculations of the simple shear flow around a single particle between two moving walls

By H. NIRSCHL[1], H. A. DWYER[2] AND V. DENK[1]

[1] Technische Universität München, Lehrstuhl für Fluidmechanik und Prozeßautomation, 85350 Freising, Germany

[2] University of California, Davis, Mechanical and Aerospace Engineering, Davis, CA 95616, USA

(Received 7 October 1993 and in revised form 21 July 1994)

Three-dimensional solutions have been obtained for the steady simple shear flow over a spherical particle in the intermediate Reynolds number range $0.1 \leqslant Re \leqslant 100$. The shear flow was generated by two walls which move at the same speed but in opposite directions, and the particle was located in the middle of the gap between the walls. The particle–wall interaction is treated by introducing a fully three-dimensional Chimera or overset grid scheme. The Chimera grid scheme allows each component of a flow to be accurately and efficiently treated. For low Reynolds numbers and without any wall influence we have verified the solution of Taylor (1932) for the shear around a rigid sphere. With increasing Reynolds numbers the angular velocity for zero moment for the sphere decreases with increasing Reynolds number. The influence of the wall has been quantified with the global particle surface characteristics such as net torque and Nusselt number. A detailed analysis of the influence of the wall distance and Reynolds number on the surface distributions of pressure, shear stress and heat transfer has also been carried out.

1. Introduction

This investigation is concerned with the flow over a spherical particle in shear flow between moving walls, which is of fundamental interest in many engineering applications. Clift, Grace & Weber (1978) give an extensive review of theoretical and experimental work on bubbles, drops and particles, and in much of the previous work the particle has been subjected to a uniform flow and/or low shear rates. Recent progress in numerical methods and computer hardware has made it possible to extend detailed numerical studies to three-dimensional flows. Dandy & Dwyer (1990) investigated the fundamental flow over a sphere in shear, and succeeded in confirming Saffman's analytic work on the lift of a particle. However, in many practical flows the particle moving with the fluid is more realistic. For this flow the particle is subjected to a simple shear flow with a positive flow at the top of the particle and a negative flow at the bottom. Taylor (1932), Rumscheidt & Mason (1961) and Bartok & Mason (1958) did extensive analytic and experimental work on Stokes flows, but they did not include inertia effects in the calculations.

We have investigated the flow around a spherical particle which is subjected to a Couette flow between two moving walls, and we have considered large as well as small gap widths. For a large gap width the flow field will simulate a particle moving in a shear field, and for a small gap width the influence of the wall will be strong. We have

also studied the influence of particle rotation, and for all flows the torque coefficient has been determined.

The three-dimensional Navier–Stokes equations have been solved with a finite volume numerical formulation which includes the thermal energy equation. The complex geometry introduced by the particle and wall has been treated with a three-dimensional Chimera grid scheme. The Chimera grid approach allows the treatment of multiple body configurations, and it allows each component of the flow to be gridded separately and overset onto a main grid. Typically, there is a main grid which in our case is a simple rectangular grid stretched over the entire gap between the two moving walls. A minor grid is generated about the particle to resolve the flow around it and the regions of high gradients. The fundamental ideas of the Chimera grid scheme approach are described by Benek *et al.* (1985), Buning *et al.* (1988) and Dougherty (1985), and the majority of previous applications have been to aerodynamic flows.

2. Problem statement and numerical approach

We begin by considering a particle at temperature T_p held fixed in the middle of a Couette flow at temperature T_∞ between the two moving walls with a gap width $2h$, figure 1. The particle is spherical with a diameter D and rigid with no slip at the surface. The two walls create a simple shear flow with the shear gradient γ. The particle can rotate with fixed angular velocity ω, and we further assume that the fluid is incompressible with a constant density ρ and dynamic viscosity μ. Each element in the geometry is associated with a boundary-fitted coordinate system. The curvilinear coordinates ζ, η and ξ with no index are used to describe the major mesh in the gap, and the boundary-fitted coordinate system ζ_1, η_1, and ξ_1 describes the mesh of the particle.

The Reynolds number Re for this flow is defined by the shear gradient γ as

$$Re = \rho\gamma D^2/\mu.$$

The flow equations are the incompressible Navier–Stokes momentum equations, continuity, and the thermal energy equation in integral form. The equations are non-dimensionalized using the diameter D of the particle as a characteristic length, γD as a characteristic velocity, $T_p - T_\infty$ as a characteristic temperature difference, and $\rho(\gamma D)^2$ as the pressure scale. The dimensionless forms of the governing equations are

$$\iint_S V \cdot \boldsymbol{n}\,\mathrm{d}A = 0,$$

$$\frac{\partial}{\partial t}\iiint_V V\,\mathrm{d}V + \iiint_V V \cdot \nabla V\,\mathrm{d}V = -\iint_S p\boldsymbol{n}\,\mathrm{d}A + \frac{1}{Re}\iint_S \boldsymbol{n}\cdot\tau\,\mathrm{d}A,$$

$$\frac{\partial}{\partial t}\iiint_V T\,\mathrm{d}V + \iiint_V V \cdot \nabla T\,\mathrm{d}V = \frac{1}{Re\,Pr}\iint_S (\nabla T)\cdot\boldsymbol{n}\,\mathrm{d}A,$$

where the velocity vector is $V = u\hat{\imath} + v\hat{\jmath} + w\hat{k}$, corresponding to the Cartesian coordinate components, p is the dynamic flow pressure, τ the viscous stress tensor, and T temperature. The Prandtl number is $Pr = \nu/\alpha$, with ν the kinematic viscosity and α the thermal diffusivity. The Nusselt number for the particle is defined by

$$Nu = \frac{1}{A_s(T_p - T_\infty)}\iint_S \nabla T \cdot \boldsymbol{n}\,\mathrm{d}A,$$

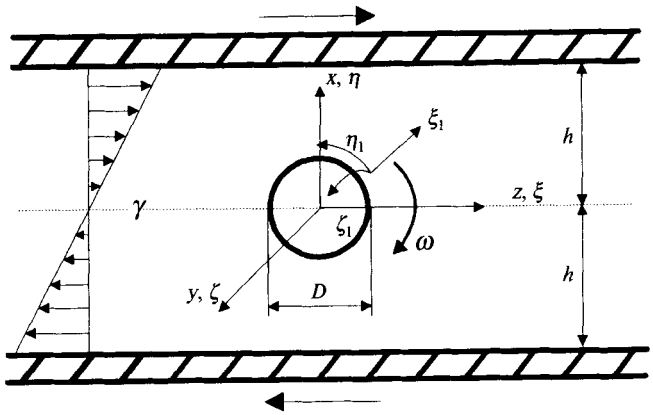

FIGURE 1. Schematic description of the problem.

with A_s the surface area of the particle. For a simple shear flow with the two walls moving with the same speed in opposite directions there is neither a drag nor a lift force on the particle owing to symmetry and no net flow in the gap.

Another important quantity for this problem is the torque on the particle caused by the shear flow. The torque coefficient, c_t is defined as

$$c_t = \int\int_S \frac{\boldsymbol{F}_t \times \boldsymbol{r}}{\frac{1}{2}\rho(\gamma D)^2 \pi D^3/8},$$

where $\boldsymbol{F}_t \times \boldsymbol{r}$ is the local torque on the particle caused by the tangential projection of the fluid forces on the surface. We have also studied the distribution of the pressure, shear stress, and heat transfer over the surface of the sphere. The shear stress tensor has been calculated with all nine components at each point on the surface, and the force vector has been determined from the stress tensor by the following relationship

$$\begin{vmatrix} \tau_{xx} & \tau_{yx} & \tau_{zx} \\ \tau_{xy} & \tau_{yy} & \tau_{zy} \\ \tau_{xz} & \tau_{yz} & \tau_{zz} \end{vmatrix} \cdot \begin{vmatrix} \mathrm{d}A_x \\ \mathrm{d}A_y \\ \mathrm{d}A_z \end{vmatrix} = \begin{vmatrix} F_x \\ F_y \\ F_x \end{vmatrix},$$

where $\mathrm{d}A_x$, $\mathrm{d}A_y$ and $\mathrm{d}A_z$ are the three components of the area normal vector. The force vector (F_x, F_y, F_z) was divided into tangential and normal components. The dimensionless pressure p, shear stress τ, and local Nusselt number Nu_1 are defined in the following way

$$p = \frac{p^+ - p_\infty}{\rho(\gamma D)^2}, \quad \tau = \frac{\tau^+}{\rho(\gamma D)^2}, \quad Nu_1 = \frac{\partial T/\partial n}{(T_p - T_\infty)/D}.$$

The solution algorithm for the equations is described in detail by Dwyer (1989), and it will only be briefly outlined here. The three velocity components and the temperature are marched in time using an implicit predictor/corrector scheme along alternating coordinate directions. The pressure change or correction algorithm consists of solving a Poisson equation derived from the continuity equation. In general it can be said that the stability and convergence properties of the numerical method are similar to single mesh calculations. However, there has been an approximate 30–50% increase in the number of time iterations needed for convergence, and this is primarily due to the transfer of information between meshes. In this work we have used second-order

central differences everywhere, and an artificial viscosity has not been introduced into the numerical method. However, at higher Reynolds numbers it may be necessary to introduce smoothing techniques if grid resolution requirements become excessive. All the calculations can be performed on a 80486 based Personal Computer with 16 MB of memory. For steady-state solutions 600 time iterations are typically taken with a non-dimensional viscous time step of 0.001, which increased by 3% until a maximum value of 0.01. (Note: dimensionless time is defined as $t = (t^+\nu)/D^2$ with t^+ as the real time.)

3. The Chimera grid scheme approach

In the Chimera grid approach the grid generation is simplified in that individual particle grids are generated independently and superimposed over the main mesh. All grids are structured in the computational space, and structured grids lend themselves to implicit algorithms which have good convergence properties with the full Navier–Stokes equations. The main grid is rectangular, and the minor grid is body fitted to the particle. The grids are stretched in all three directions of the coordinate system to improve resolution near boundaries and/or interesting flow features.

Figure 2 shows a typical Chimera grid configuration in the symmetry plane of the particle problem under consideration. In this example the walls are very close to the particle, and the main mesh is refined close to the walls to resolve high gradients caused by particle–wall interactions. For the particle grid we have chosen a spherical mesh which is refined in the radial direction to resolve the flow near the surface of the particle. Other geometries are not excluded, and it is also possible to study more complex particle geometries with the use of hyperbolic or elliptic grid generators.

The typical Chimera scheme can be divided into two major parts:

(i) *Determination of the holes and fringe points*

The holes are the points in the major mesh where the rigid body is located, and these points must be excluded from the solution procedure. In figure 2 the holes are marked with the open squares, and the solution solver skips these points with the use of an integer flag set to zero for holes. The holes also can exist in the minor mesh, and this occurs when points in the minor mesh are located outside the main grid region.

The solution variables of the two meshes are exchanged at special points, which completely enclose the holes. These special points are called 'fringe points', and they serve as the final points on the mesh where information is transmitted between the two grids. In the computer code itself they are treated like boundary conditions. In figure 2 the fringe points are marked with the filled squares, and the solution values are determined by three-dimensional interpolation from the minor grid cell where the fringe points are located.

(ii) *The interpolation scheme*

An important feature of the Chimera method is its ability to accurately interpolate the solution from one mesh to another at the fringe points. This is accomplished with the use of trilinear interpolation in the *logical space* of the body-fitted coordinate system (ζ, η, ξ). The logical space, integer-*ijk*, is cubical while the physical space is curved, and the relationship between the two is nonlinear. A difficult part of the interpolation is to find the logical space location of the fringe point in the other mesh. The location has been found with the use of Newton's method to solve the defining nonlinear simultaneous equations. With the location known, it is then a simple

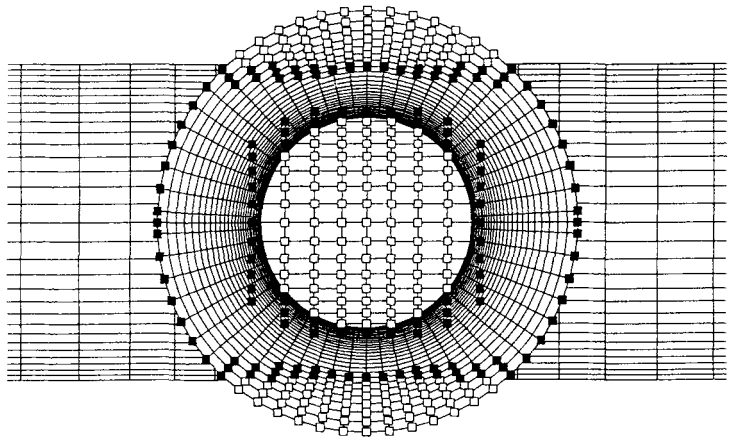

FIGURE 2. Typical Chimera grid configuration.

procedure to interpolate between grid points without the inversion of matrices to solve the simultaneous equations. The detailed procedure is described by Nirschl, Dwyer & Denk (1993).

The logical space coordinates for the fringe points are only calculated once at the beginning of the solution procedure. For a more difficult simulation with particle movement in a flow we have only to recalculate the location of the holes and fringe points. This is a significant advantage, since a remeshing is not necessary as the particle moves. A full simulation of the flow around a moving particle array will be feasible in the near future.

The first validation of our Chimera scheme has been for a three-dimensional heat transfer problem in a square geometry where an exact solution exists. We have solved this problem with different numbers of grid points (from $21 \times 21 \times 21$ up to $41 \times 41 \times 41$), different minor meshes (orthogonal and non-orthogonal) located in the middle of the major mesh, and different numbers of holes, and the single and Chimera mesh solutions were identical to better than four significant figures. In general, overlap between two grids is very useful, and our experience has shown that the holes of the major mesh should be at least four to five grid points within the minor mesh for good convergence properties.

Another test problem was the well-known solution for the axisymmetric flow over a sphere in an unbounded fluid for Reynolds numbers in the range ($0.1 \leqslant Re \leqslant 100$). The main grid was a simple rectangular one, and around the particle we have chosen a three-dimensional spherical grid. Coarse solutions have been obtained with an accuracy of 10% for the drag coefficient on a mesh of $21 \times 21 \times 21$ for both the major and the minor mesh. With $31 \times 31 \times 31$ points we have been able to reproduce the single mesh solutions in the published literature. The location of the outer boundary of the minor mesh did not have a strong effect on the solution as long as the grid density at the particle surface was high enough to resolve the gradients. In the present paper the Chimera grid scheme will be tested and verified against the analytic solution of Taylor (1932) for the Stokes flow around a single particle in simple shear.

A summary of the Chimera grid scheme approach is:

(*a*) calculation of the main and minor mesh,

(*b*) determination of the holes and fringe points,

(*c*) determination of the fringe point locations in logical space for use with trilinear interpolation,

(*d*) iteration of the system of equations on the minor mesh,

(*e*) interpolation of the variables of the minor mesh to the fringe points in the major mesh,

(*f*) iteration of the system of equations in the major mesh,

(*g*) interpolation of the variables of the major mesh to the fringe points in the minor mesh,

(*h*) repeat steps (*d–g*) until the solution is converged.

4. Results and discussion

4.1. *Taylor's solution for Stokes flow*

For low Reynolds number flow over a rotating sphere in simple shear the solution has been obtained analytically by Taylor (1932), and Taylor's results have been verified by the experiments and extensions of Rumscheidt & Mason (1961). An important result is the distribution of shear and normal stresses on the surface of the sphere, and the shear stress distribution in the symmetry plane is given as

$$f_s = \tfrac{5}{2}\mu\gamma\cos 2\theta,$$

where the angle θ is measured from the sphere rear stagnation point. The normal stress distribution is

$$f_n = \tfrac{5}{2}\mu\gamma\sin 2\theta$$

and the solution is for a particle rotating with a dimensionless angular velocity of one half. For this angular velocity the net torque on the particle is zero.

We have calculated this flow for a Reynolds number, $Re = 0.1$, and with a gap width of forty times the particle radius. A mesh of $31 \times 31 \times 41$ grid points has been used in the main mesh and $31 \times 31 \times 31$ points in the minor mesh. A comparison of the surface normal stress (pressure) distribution is shown in figure 3(*a*) for the numerical and the Taylor solution, and the agreement is good. The differences between the numerical and analytic values are less than 4%, and further improvements can be obtained by decreasing the Reynolds number in the calculations or by increasing the number of grid points in the angular direction. With the present numerical method it requires more iterations for low Reynolds number flow than at higher Reynolds number. This is due to the strong coupling in space between pressure and velocity, and the very diffusive nature of low Reynolds number flow. In some flows it may require as much as five times the number of iterations to obtain a fully converged result for the same geometry at very low Reynolds number.

A similar comparison with the shear stress is given in figure 3(*b*), and again the agreement is quite good. The distributions are antisymmetric between the front and the back side of the particle, and the three-dimensional solution is very smooth with all gradients sufficiently resolved. A more detailed discussion of these three-dimensional distributions is given later in this paper, where the higher Reynolds number results are presented.

4.2. *Influence of the walls*

We next study the influence of the walls on the flow around the particle. An important feature of the flow is that there is not a net flow in the gap, and this implies that the net drag and lift are zero. Therefore, it is not possible to use the drag and lift as criteria for evaluating the influence of the walls on the flow around the particle. We have therefore decided to use the Nusselt number Nu, the non-dimensional torque times the Reynolds number $c_t\,Re$, and the maximum surface stagnation pressure p_{max} as flow

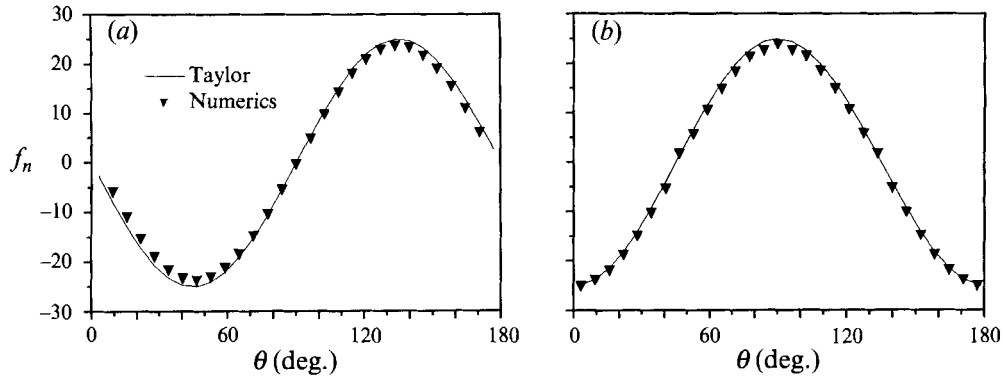

FIGURE 3. (*a*) Normal stress and (*b*) shear stress distributions around a sphere: comparison with Taylor's (1932) results.

indicator variables. The variable $c_t Re$ was chosen for a better presentation of the results, since a logarithmic scaling of c_t over h does not allow the presentation of positive and negative torques, and an arithmetic scaling is very sensitive to small changes of Reynolds number. The calculated results cover the range of gap widths of an order of magnitude, from $h = 7.5$ to 0.75. For many practical applications it would be of interest to study the flow when the walls are close or placed on the particle surface; however, this problem would require a new interpolation technique for complex control volumes between the particle and wall. Figure 2 shows the grid that was used for $h = 0.75$, and where there are significant regions of both holes and fringe points in the main and particle meshes. In figure 2 the outer boundary of the minor grid was reduced to two times the particle radius in order to obtain a better resolution between the particle and the wall. This refinement did not have an effect on the particle global characteristics, and for other gap widths the outer boundary was at three times the particle radius.

The variation of Nusselt number with Reynolds number and wall gap for a non-rotating particle is presented in figure 4(*a*). The influence of the walls on the flow around a particle which is non-rotating is the most dramatic. For a low Reynolds number flow, $Re = 0.1$, we obtain the maximum sensitivity to the wall gap; however, for the walls far away we obtain a solution very close to pure heat conduction around a spherical particle in an unbounded fluid. The value of the Nusselt number, $Nu = 2.18$, is consistent with a Reynolds number of 0.1, and it can be further lowered by using a smaller Reynolds number. As the walls come closer to the particle the Nusselt number increased owing to the direct conduction between the walls and the particle. For small values of h there is direct heat conduction path between the wall and the particle, and this wall conduction effect is very important. It should be noted that the result curves become very close as the wall approaches the surface of the particle for the lower Reynolds numbers. At a higher Reynolds number of 100 the walls have only a weak influence on the Nusselt number, because the flow is dominated by the convection over the particle surface.

Figure 4(*b*) presents the non-dimensional torque $c_t Re$ for the non-rotating particle, and we obtain relatively large values for the torque. (Note: the particle torque is defined positive counterclockwise.) The torque dependence implies that the rotation speed of a particle in pure shear flow must be a function of the Reynolds number. The quantitative dependence on Reynolds number and gap width is not very strong;

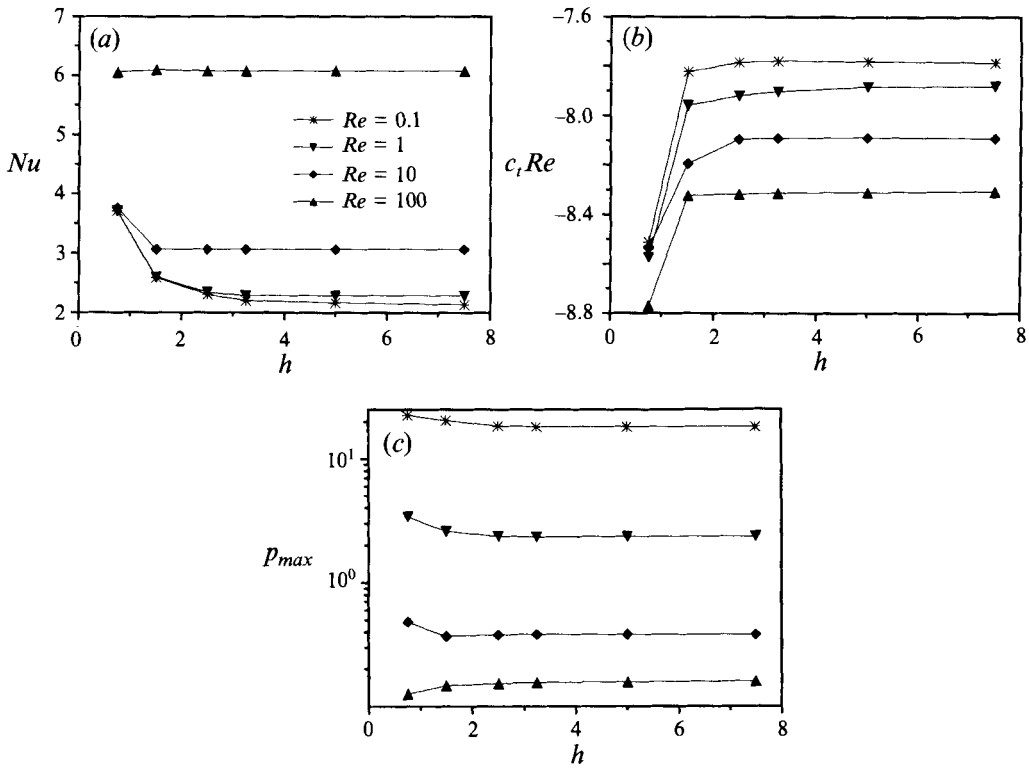

FIGURE 4. (*a*) Nusselt number Nu and (*b*) non-dimensional torque coefficient $c_t Re$ as a function of wall distance h, $\omega = 0$. (*c*) Maximum stagnation pressure p_{max} as a function of wall distance h.

however, its behaviour is complex owing to particle blockage. The influence of the walls on the low Reynolds number flows is more significant.

A variable that is sensitive to the flow field is the maximum dimensionless pressure on the particle surface, figure 4(*c*). For a high Reynolds number the maximum surface pressure decreases with decreasing gap width, and for a non-rotating particle we have an important blockage effect along the centreline region of the particle. This blockage creates a recirculation of fluid, and the streamlines are diverted into the gap. Thus the resistance to the flow in the gap increases, and the flow losses are larger. As the wall moves closer to the particle this effect is more important, and the recirculation region causes a lowering of the maximum surface pressure. (Note: the low values of pressure in figure 4(*c*) are partially due to the definition of dimensionless pressure.)

4.3. *Influence of particle rotation*

The influence of particle rotation will be limited to values of a wall gap less than 3.75, since the previous non-rotating results clearly show that the wall influence is weak for larger values of h. Figure 5(*a*) shows the dependence of the Nusselt number on the Reynolds number when the walls are not important, and we have chosen three angular velocities, $\omega = 0$, 0.5, and 1.0. The angular velocity influence on Nusselt number is only significant at the larger Reynolds numbers, and the effect is not a strong one. Another feature of the results is that the lowest heat transfer occurs for the fastest rotation, and this result is caused by particle rotation spreading surface fluid over the particle, which will insulate the particle. At higher Reynolds numbers it may be possible to obtain other possibilities due to flow separation.

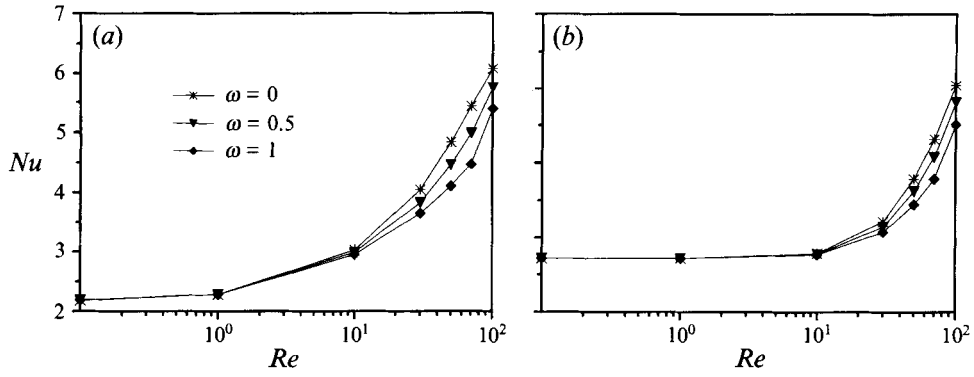

FIGURE 5. Nusselt number Nu as a function of Reynolds number Re with (*a*) $h = 3.75$, and (*b*) $h = 0.75$.

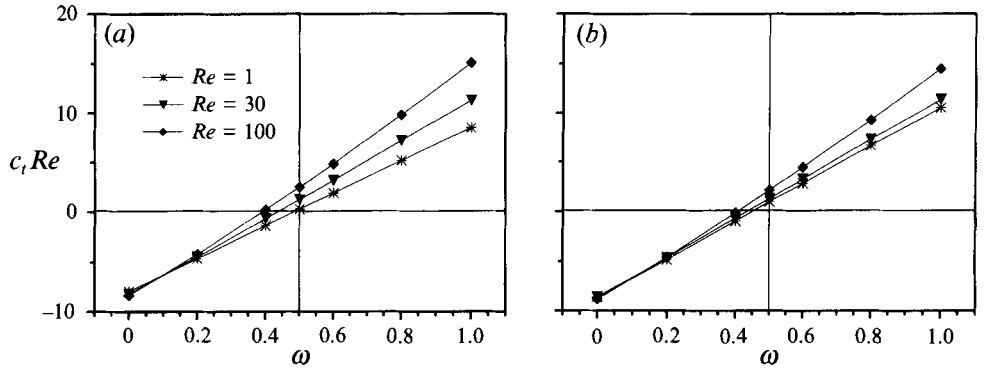

FIGURE 6. Non dimensional torque coefficient $c_t Re$ as a function of angular velocity ω with (*a*) $h = 3.75$, and (*b*) $h = 0.75$.

As the walls are moved closer to the particle surface the influence of rotation on the Nusselt number is not as strong, figure 5(*b*). The Nusselt number remains almost constant for values lower than $Re \leqslant 10$, and the rate of heat transfer is dominated by the distance from the walls. Compared to figure 5(*a*) the heat transfer for low Reynolds numbers is higher owing to the conductive influence of the two walls. With increasing Reynolds number the wall influence is negligible on the heat transfer around the particle.

We will now show the non-dimensional torque $c_t Re$ on the particle as a function of angular velocity and Reynolds number. Figure 6(*a*) presents the torque coefficient when the walls are far away from the surface at $h = 3.75$. In the figure the Reynolds number is a parameter, and for an angular velocity of one half the torque approaches the lowest value. This result is similar to Taylor's solution; however, these results do differ from the low Reynolds number solutions. For high Reynolds numbers the particle does not rotate with zero torque at an angular velocity of one half, and the curves in figure 6(*a*) indicate that the zero-torque position moves to lower values of angular velocity. When the particle is rotating at a higher angular velocity the dependence of the torque on the Reynolds number is much stronger than when the particle is fixed in the flow. For low Reynolds numbers the dependence is almost linear while at higher ones the nonlinear convective influence becomes more important.

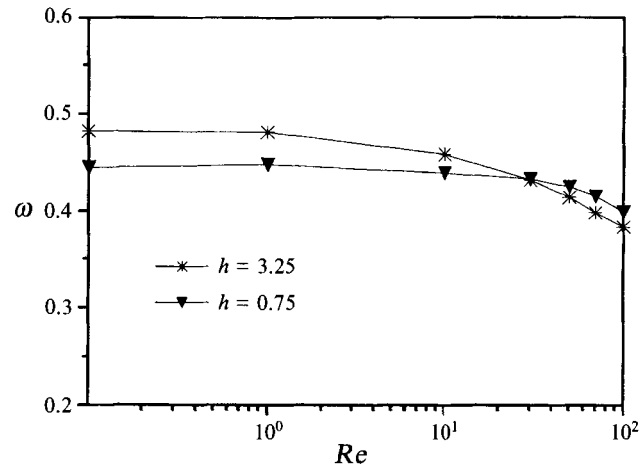

FIGURE 7. Angular velocity ω as a function of Reynolds number Re.

As the wall is moved closer to the particle the largest impact is felt for the low Reynolds number flow, and the results are shown in figure 6(*b*) for $h = 0.75$. At the lower Reynolds numbers the wall is the dominant influence and the torque coefficient is almost constant with the angular velocity. A detailed analysis of the data has shown that the isolated particle has a larger torque coefficient at the higher Reynolds numbers, and this is explained in the next paragraph.

An important result is the angular velocity for which zero torque is obtained on the particle. This angular velocity, ω, is given as a function of Reynolds number in figure 7 for $h = 0.75$ and 3.75. For the larger gap the angular velocity approaches the Taylor result of one half, although the result is slightly different from one half due to the combined influences of the walls, finite Reynolds number, and truncation error. At a gap width of $h = 0.75$ there is a 10% shift in angular velocity to lower values, and this increases slowly with Reynolds number. The reason for this effect is blockage of fluid near the particle axis. The fluid blockage creates a recirculation of fluid, and the streamlines are diverted into the gap. The resistance to flow in the gap increases, and the flow losses are larger. For the low Reynolds numbers the blockage arises purely from the walls close to the particle surface. The blockage is also visible when the Reynolds number increases, and when the flow is not influenced by the walls.

The recirculation comes from convective effects and the separation of the flow on the back sides of the particle. The effect is not so important for small wall distances since recirculation is inhibited. This behaviour is the reason for the transition of the two curves in figure 7. At the higher gap width the sensitivity to Reynolds number is greater, and we obtain the result of a bigger shift in the zero torque angular velocity for a larger gap.

4.4. *Three-dimensional distribution of the surface stresses and heat transfer*

In this section we will present a three-dimensional distribution of flow variables at the surface of the particle. Surface pressures and stresses are of interest in applications concerning the structural stability of particle systems. In order to be able to handle the large amount of data it is necessary to develop new graphical tools to fully comprehend the solution. In recent years the use of graphics has progressed rapidly, and we have been able to write our own graphics routines. The distributions of the dimensionless stresses, pressure and heat transfer as contours of constant values are shown over the

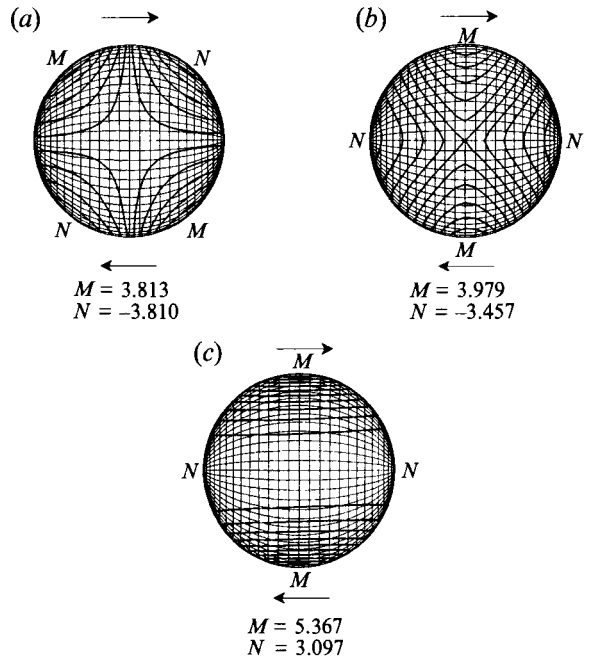

FIGURE 8. Contours at the surface of the particle for $Re = 1$, $\omega = 0.5$, $h = 0.75$: (*a*) pressure, (*b*) shear stress, (*c*) heat transfer.

particle surface. The contours are linearly distributed between the maximum and minimum values, and these plots give a better understanding of the force distribution at the particle surface. For the presentations we have chosen a Reynolds number $Re = 1$ at a wall distance of $h = 0.75$ (figure 8) and $Re = 100$ at $h = 3.75$ (figure 9), and we will also allow the particle to rotate at an angular velocity of one half.

Figure 8(*a*) shows the pressure contours at the surface of the sphere for a Reynolds number of one, and the flow directions are marked with vectors. At the top of the picture the flow goes from left to right, and the maximum and minimum values for the variables are marked M and N (the numerical values are also given). The pressure contours are symmetric around the particle axis with two corresponding maximum and minimum values. The high-pressure regions are located on the upstream sides with the high pressure in the middle of the sphere. At a Reynolds number of 100 (figure 9*a*) the pressure contours have a totally different shape compared to pure viscous flow. The largest effect has been on the pressure minimum, and this is directly due to the acceleration of the fluid over the sphere, and the low-pressure regions are shifted towards the front side of the particle. The low values of non-dimensional pressure reflect the definition of Reynolds number and large losses in the flow.

The shear stress contours for the low Reynolds number flow also have a high degree of symmetry, and the maximum values are on the high-velocity sides of the sphere (figure 8*b*). The maximum shear stress occurs in the regions where the flow tries to accelerate the particle, while in the regions of minimum shear stress the particle speeds up the fluid. For the high Reynolds number case (figure 9*b*) the maximum and minimum values are shifted, again due to the acceleration of the flow around the particle. There is also a normal component of the viscous stress tensor resulting from the rotation of the particle. For a fixed particle we do not have any normal viscous component, while for a rotating particle the viscous normal force will not vanish. In

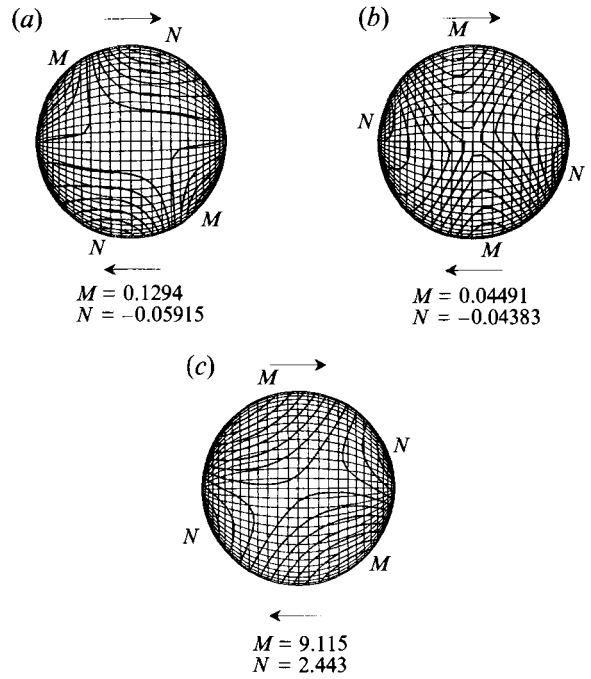

FIGURE 9. Contours at the surface of the particle for $Re = 100$, $\omega = 0.5$, $h = 3.25$: (*a*) pressure, (*b*) shear stress, (*c*) heat transfer.

the Taylor solution the flow is dominated only by the viscous forces and there are no effects of inertia. For $Re = 1$ the magnitude of the normal stress increases to almost 20% of the viscous shear stress. At higher Reynolds numbers the influence of the viscous normal stresses on the stress distribution will decrease since the flow is strongly dominated by convection over the particle. The inertia effects caused by the particle rotation are much less than those caused by the convection over the particle surface. The distribution of normal viscous stresses looks similar to the pressure distribution; however, the minimum and maximum values are interchanged.

When the walls are close to the particle surface for a low Reynolds number the distribution of the pressure and viscous stress contours at the surface do not qualitatively change; however, the absolute values increase, the maximum as well as the minimum. The most significant changes were visible in the local Nusselt number distribution over the particle. The heat transfer distribution for a low Reynolds number flow is essentially constant over the surface when the walls have no influence. When the channel walls are close to the particle surface there is a definite trend toward one-dimensional heat transfer in the channel (figure 8*c*). The local values have increased, with a considerable difference between the maximum and minimum values.

For higher Reynolds numbers (figure 9*c*) the contours show a quite different behaviour. As expected the local Nusselt number on the surface has increased with significant maximum and minimum values. For the high Reynolds numbers the influence of the walls is negligible in the range of this investigation. This reflects the domination of the convection terms in the flow, which are not significantly changed by the walls, even when they are close to the particle surface.

5. Conclusions

The main conclusions of the paper are the following.

(i) A fully three-dimensional Chimera grid scheme was successfully implemented into an incompressible Navier–Stokes computer code for the calculation of particle flows. In this study the flow over a rotating particle in Couette flow with varying wall distance was investigated.

(ii) With the help of the Chimera grid scheme approach it was possible to study the effects of particle–wall interaction on the global variables like Nusselt number and dimensionless torque. The most significant changes have been observed on the behaviour of the Nusselt number verses the distance of the walls to the particle surface.

(iii) The zero-torque angular velocity of the particle in shear flow depends on the Reynolds number. With increasing Reynolds number the angular velocity of the particle is decreasing for the zero-torque condition.

(iv) A detailed study of the forces and the heat transfer distribution at the surface of the particle shows some significant influences of the walls. The effects depend very strongly on the Reynolds number, or whether the flow is dominated by convection or diffusion of momentum and heat.

REFERENCES

BARTOK, G. & MASON, S. G. 1958 Particle motions in sheared suspensions. *J. Colloid Sci.* **13**, 293.

BENEK, J. A., STEGER, J. L., DOUGHERTY, F. C. & BUNING, P. G. 1985 Chimera: A grid-embedding technique. *AEDC-TR*-85-64. NASA Ames Research Center.

BUNING, P. G., CHIU, I. T., OBAYASHI, S., RIZK, Y. M. & STEGER, J. L. 1988 Numerical simulation of the integrated space shuttle vehicle in ascent. *AIAA Atmospheric Flight Mechanics Conf., Minneapolis, Minnesota, AIAA*-88-4359-CP.

CLIFT, R., GRACE, J. R. & WEBER, M. E. 1978 *Bubbles, Drops and Particles.* Academic Press.

DANDY, D. S. & DWYER, H. A. 1990 A sphere in shear flow at finite Reynolds number: effect of shear on particle lift, drag and heat transfer. *J. Fluid Mech.* **216**, 381.

DOUGHERTY, F. C. 1985 Development of a Chimera grid scheme with applications to unsteady problems. PhD thesis, Stanford University.

DWYER, H. A. 1989 Calculations of droplet dynamics in high temperature environments. *Prog. Energy Combust. Sci.* **15**, 131.

NIRSCHL, H., DWYER, H. A. & DENK, V. 1993 A Chimera grid scheme for the calculation of particle flows. *J. Comput. Phys.* (Submitted).

RUMSCHEIDT, F. D. & MASON, S. G. 1961 Deformation and burst of fluid drops in shear and hyperbolic flow. *J. Colloid Sci.* **16**, 238.

SAFFMAN, P. G. 1965 The lift on a small sphere in a slow shear flow. *J. Fluid Mech.* **31**, 385.

TAYLOR, G. I. 1932 The viscosity of a fluid containing small drops of another fluid. *Proc. R. Soc. Lond.* A **138**, 41.